Controlling the Velocity of Jumping Nanodroplets *Via* Their Initial Shape and Temperature

Miguel Fuentes-Cabrera,[†,*] Bradley H. Rhodes,[‡] Michael I. Baskes,[§] Humberto Terrones,[†] Jason D. Fowlkes,[†] Michael L. Simpson,[†,⊥] and Philip D. Rack[†,⊥,*]

[†]Center for Nanophase Materials Sciences, and Computer Sciences and Mathematics Division, Oak Ridge National Laboratory, P.O. Box 2008, Oak Ridge, Tennessee 37831-6494, United States, [‡]Department of Electrical Engineering and Computer Sciences, University of Tennessee, Knoxville, Tennessee 37996, United States ., [§]Los Alamos National Laboratory, MST-8 MS G755, Los Alamos, New Mexico 87545, United States, and [⊥]Materials Science and Engineering Department, University of Tennessee, Knoxville, Tennessee 37996, United States

ABSTRACT Controlling the movement of nanoscale objects is a significant goal of nanotechnology. Dewetting-induced ejection of nanodroplets could provide another means of achieving that goal. Molecular dynamics simulations were used to investigate the dewetting-induced ejection of nanoscale liquid copper nanostructures that were deposited on a graphitic substrate. Nanostructures in the shape of a circle, square, equilateral, and isosceles triangle dewet and form nanodroplets that are ejected from the substrate with a velocity that depends on the initial shape and temperature. The dependence of the ejected velocity on shape is ascribed to the temporal asymmetry of the mass coalescence during the droplet formation; the dependence on temperature is ascribed to changes in the density and viscosity. The results suggest that dewetting induced by nanosecond laser pulses could be used to control the velocity of ejected nanodroplets.

KEYWORDS: molecular dynamics simulations · dewetting · copper · graphite · nanodroplets

Guiding a nanoparticle toward a tumor by using external magnetic fields, synthesizing a nanorotor from a metal plate and a multiwalled carbon nanotube,[1] or building a nanomachine out of nanosize moveable parts[2] are only some of the important applications that controlling and guiding the movement of nanoscale objects can provide. Laser-induced ejection of nanoparticles could offer one more possibility toward controlling the movement of nanoparticles.

Recently, Habenicht *et al.*[3] and Huang *et al.*[4] have shown that Au triangles deposited on a substrate can be vertically ejected when they are heated up with nanosecond or femtosecond laser pulses, respectively. The process that leads to ejection is different in these experimental studies. In Habenicht *et al.*,[3] the ejection is caused by dewetting: heating leads to the melting and then dewetting of the triangles, which contract and form nanodroplets; during the contraction, the center of mass moves upward and detachment occurs due to inertia. In Huang *et al.*,[4] there is not enough time for melting to take place, dewetting does not occur, and the triangles do not deform; the triangles remain triangles before and after lift-off. Au ablation, instead of dewetting, drives the detachment: ablation leads to a buildup of pressure in the interface between the Au triangle and the substrate, and when this pressure is large enough, the triangle is vertically ejected. This process is referred to as laser-induced forward transfer or LIFT.[5]

During the past few years, we have investigated laser-induced dewetting of metallic nanostructures as a means to self-assemble functional nanoparticles.[6−12] It was during our efforts in this area that we started to consider whether it would be possible to control, and then guide, the ejection of nanoparticles by changing the nanostructure's initial shape. What led us to this consideration was the following. On one hand, in ref 13, we carried out a theoretical study based on a molecular dynamics (MD) simulations to investigate the dewetting of Cu liquid disks and lines deposited on graphite. We described the Cu−C interaction with a 12-6 Lennard-Jones (LJ) potential that was fitted to *ab initio* and experimental data. When this potential was used to model the dewetting of Cu disks on graphite, we found that the disks not only dewetted, contracting into nanodroplets, but also were ejected from the graphitic substrate. The ejection velocity was on the order of 100 m/s. Qualitatively, our results mimicked very well the experimental findings of Habenicht *et al.*[3] and encouraged us to use MD simulations to study metallic thin film dewetting phenomena that lead to the ejection of nanoparticles. MD simulations have been successfully

* Address correspondence to fuentescabma@ornl.gov, prack@utk.edu.

Received for review May 18, 2011 and accepted July 31, 2011.

Published online August 01, 2011
10.1021/nn2018254

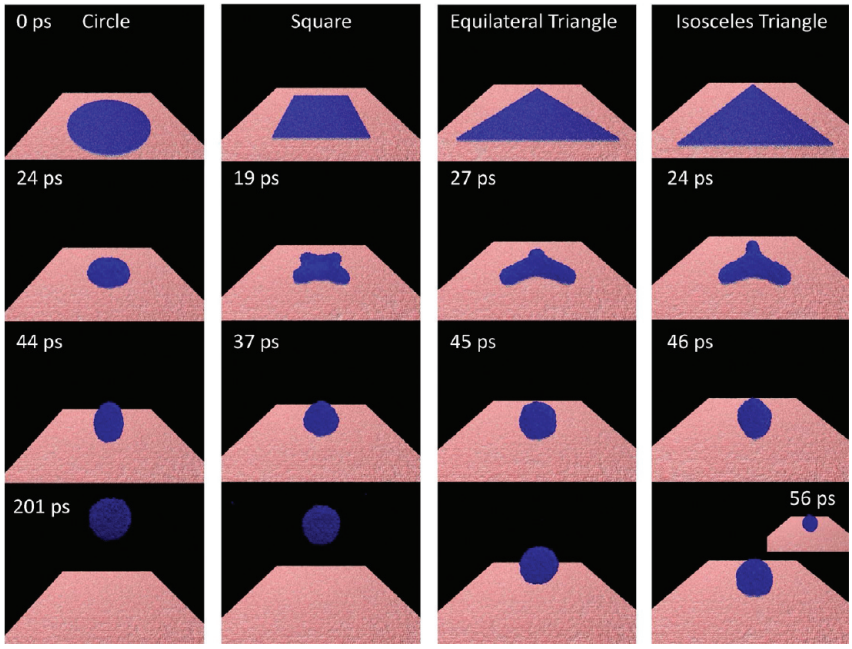

Figure 1. Snapshots of the different shapes simulated at 1900 K (tilted at 70°). The top row is the original liquid Cu nanostructures (blue atoms) on the graphitic substrate (pink atoms). All of the areas are equal to ~45239 Å^2, and thus the dimensions of the shapes are as follows: the circle has a radius of 120 Å; the length of the square is 212.7 Å; each edge of the equilateral triangle is 323.2 Å; the isosceles triangle's small and large edges are 278.4 and 353.6 Å, respectively. The snapshots in rows 2 and 3 represent discontinuities in the displacements, and they are also indicated with symbols in Figure 4. Column 4 shows the snapshots at 201 ps, and they illustrate the position of the droplet above the substrate for all shapes except for the isosceles triangle, in which case the droplet does not jump but remains in equilibrium with the substrate.

used before to investigate the dewetting of polymer-like liquids and metallic liquids; see for example the excellent works of Koplik,[14] Bertrand, Blake and De Coninck,[15−19] and Webb *et al.*[20] and Heine *et al.*,[21] but our work was the first one to show that MD simulations can also be used to investigate the dewetting-induced ejection of nanoparticles. On the other hand, during our experimental investigations of the liquid phase assembly of different shapes, we showed that the dewetting of different shapes produces different structures. For example, we experimentally compared the dewetted rim velocities of a disk, triangle, and square[7] and showed that there is a dependence on the in-plane radius of curvature. Furthermore, we have compared the dewetting process of various isosceles triangles and showed that nanodroplets form that are positioned at the center of mass and not at the intersection of the perpendicular bisectors.[9] It seemed then plausible to propose that the initial shape could affect the ejection velocity, and that MD simulations could be used to probe this hypothesis. This is what we do here by investigating with MD the dewetting of liquid Cu nanostructures in the shape of a circle, square, equilateral triangle, and isosceles triangle that are deposited on a graphitic substrate at different temperatures, such as 1500, 1700, 1900, and 2200 K.

RESULTS AND DISCUSSION

Figure 1 shows snapshots that capture some of the dynamics of each shape during dewetting as well as nanodroplet formation and ejection from the substrate. The nanodroplet is colored according to its height. White regions indicate close proximity to the substrate, while blue regions are relatively farther from the substrate surface. Dewetting induces mass flow toward the center of mass.[9] As a result, vertices accumulate more mass (inversely proportional to the angle) than either the straight edges or the circular rim; these results are encouraging because they are in agreement with our experimental findings for the same patterned geometries of larger sizes.[7] As dewetting proceeds, the traveling rims meet at the center of the structure forming a nanodroplet. This convergence of mass coupled with the constraint of a rigid substrate surface ultimately forces mass upward, that is, away from the substrate. Consequently, the droplet elongates in the $+z$-direction which, depending on the original shape and temperature, leads to ejection from the substrate. The snapshots shown in Figure 1 were taken from the 1900 K simulations, but the same phenomena are observed at 1500, 1700, and 2200 K.

Figure 2 shows the z-component of the nanodroplet center of mass, Z_{CM}, *versus* time for each shape and temperature. For the circle and the square, after about 50 ps, and for all simulated temperatures, Z_{CM} increases linearly with time. This transition to a linear behavior was determined to indicate the detachment/ejection of the droplet from the substrate surface (see ejection times in Table 1). For the equilateral triangle, a linear increase in Z_{CM} was observed after

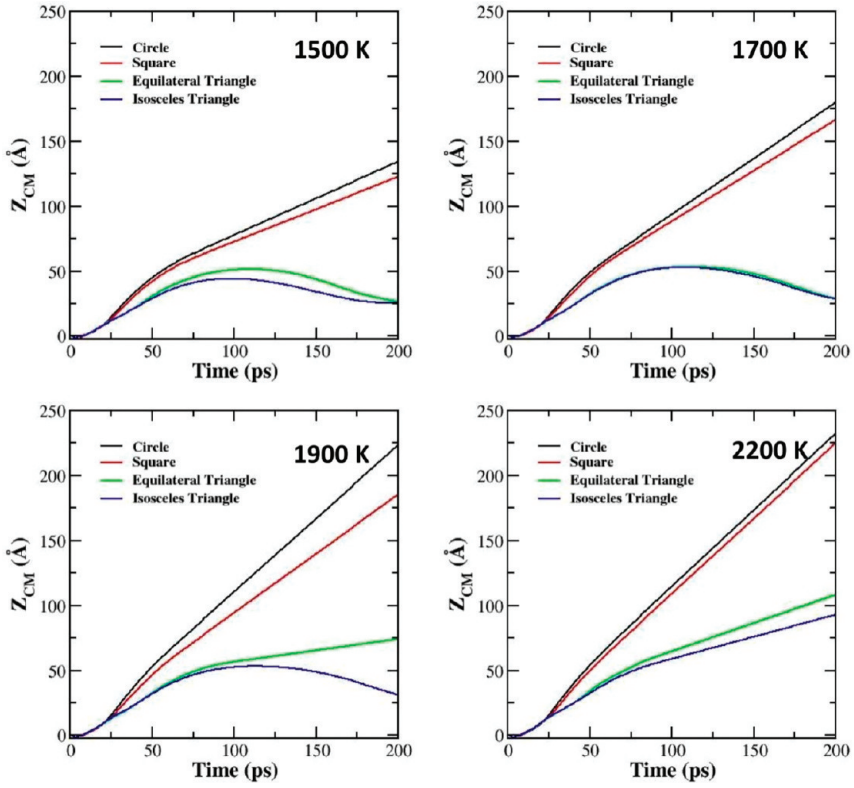

Figure 2. Vertical displacement of the center of mass (Z_{CM}) for each shape at different temperatures.

TABLE 1. Velocities (m/s)/Ejection Times (ps) at Different Temperatures for All of the Simulated Shapes[a]

shape	1500 K	1700 K	1900 K	2200 K
circle	56.59/82	86.15/72	112.96/68	117.81/72
square	50.04/83	78.14/77	91.07/73	115.89/74
equilateral			15.53/108	43.59/97
isosceles				34.08/102

[a] The velocities were computed as described in the text. The ejection times are estimations, as they were obtained by visually inspecting the times at which the nanodroplet detaches the substrate.

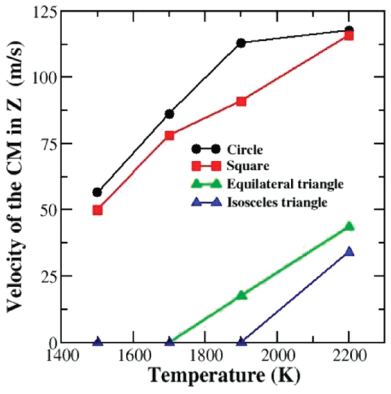

Figure 3. *z*-Component of the velocity of the center-of-mass (CM) as a function of the initial shape and temperature.

75 ps at 1900 and 2200 K. Z_{CM} increased linearly also after 75 ps but only at 2200 K for the case of the isosceles triangle. In all other cases, Z_{CM} increases and decreases in a parabolic-like manner, indicating a recoiling of the droplet, which remained attached to the substrate. From the slopes of Figure 2, we computed the ejection velocities (see Table 1), and their dependence on the initial shape and temperature is shown in Figure 3. Clearly, for all temperatures, the circle moves the fastest, followed by the square, the equilateral, and the isosceles triangle; for all shapes, the velocity increases with increasing temperature. Thus, both the initial shape and temperature affect the magnitude of the ejected velocity.

To understand the effect of temperature and shape on the ejected velocity, it was instructive to compare the energy of the initial shape to the energy of the corresponding final droplet. The initial shapes differ only on their perimeter length because their areas and thicknesses are all equal. Thus, the only difference in energy among the various initial shapes is given by their differences in the perimeter length (perimeter × thickness). As for the final droplets, their energy is independent of the initial shape if one assumes, as we do here, a final liquid spherical droplet of equal volume for all of the shapes. Ignoring viscous and contact line dissipation, one would expect the kinetic energy (and consequently the velocity of the equal mass droplets) to scale with the perimeter length. The perimeter length increases in the order: circle, square,

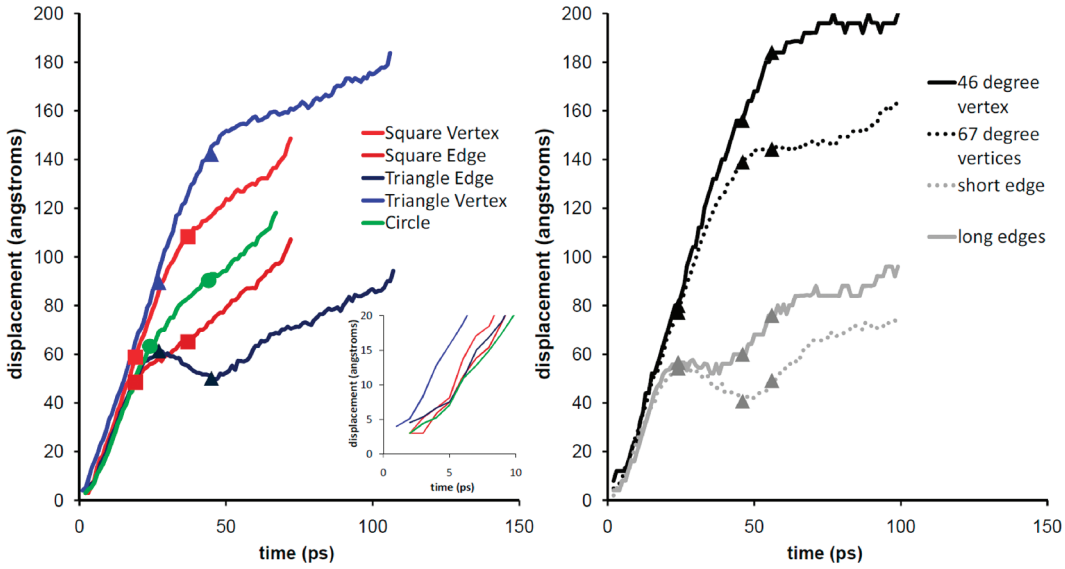

Figure 4. Simulated contact line displacement *versus* time at 1900 K for the (left) circle, square vertices and edges, and equilateral triangle vertices and edges (inset is an expanded view of early times) and (right) the isosceles triangle vertices and edges. The symbols correlate to observed discontinuities and correspond to the snapshots in rows 2 and 3 of Figure 1.

equilateral triangle, and isosceles triangle, which means that according to an energy comparison the velocities should increase in the same order. In fact, we observed the opposite trend. As a result, we examined the transport behavior of the different shapes in greater detail to discern what was leading to this counterintuitive trend.

We ascribe the dependence of the ejection velocity on shape to the temporal asymmetry of the mass coalescence during the droplet formation. Specifically, the pressure gradient that leads to a jumping nanodroplet is a function of the magnitude of the transverse velocity gradient in the coalesced nanodroplet; this pressure gradient depends on the velocity gradient in the traveling rims as well as the timing at which all of the rims coalescence. Figure 4 shows the displacement of the contact line *versus* time at 1900 K for the circle, the square edges and vertices (90°), the equilateral triangle edges and vertices (60°), and the isosceles triangle edges (long and short) and vertices (67° and 46°). The inset of of the left panel of Figure 4 shows the displacement of the contact line up to a time of ~30 ps. From the slope of this plot, the transverse velocity was computed. We call this the initial velocity. The initial velocity increases in the order: triangle and square edge, circle, square vertex, and triangle vertex. The in-plane radius of curvature slightly enhances the initial velocity, a result that is once again encouraging for it is consistent with our recent experimental studies.[9] Examination of the still images in Figure 1 correlates to some of the discontinuities noted with symbols in Figure 4 and illustrates the key observation regarding the synchronicity of the droplet coalescence and its influence on the vertical velocity. The rim of the circle, obviously, coalesces at the same time and thus maximizes the velocity component in the *z*-direction of the nanodroplet. However, for the isosceles triangle, even though the vertices travel faster, the short edge rim reaches the center first, followed by the long edges, followed by the large angle vertices and finally by the smaller angle vertex. This asynchronous coalescence results in a lower *z*-component of the velocity vector and not enough momentum for particle detachment. Figure 5 provides more evidence: it shows a color map of the average atomic velocity in the *z*-direction for atoms in 12 Å × 12 Å × 12 Å voxels at different *z*-slices at critical times in the droplet formation. Clearly, the velocity gradient is much larger in the circle (a) where the rim coalesces at the same time (24 ps) than for the equilateral triangle, for which coalescence occurs in two steps; first the rims meet at 27 ps (b), and then the vertices meet at 45 ps (c). It follows that the nanodroplet velocity difference among different shapes is related to the asynchronicity of the coalescence.

It is more difficult to untangle the dependence of the ejection velocity on temperature, but we have attempted to find a correlation with the changes in properties relevant for the transport behavior, that is, density and viscosity. In Table 2, we have collected the number of atoms and the calculated density and viscosity for the Cu circle for each of the temperature studied here. As the temperature increases, both the density and the viscosity[22] decrease. Between 1500 and 2200 K, the estimated density, and thus the mass change, decreases by 7.6%, a number that is consistent with the decrease in the number of simulated atoms, 7%. Between the same temperatures, the calculated viscosity decreases by 37%. We believe that, as temperature increases, the combination of lower density and viscosity causes an increase in the nanodroplet

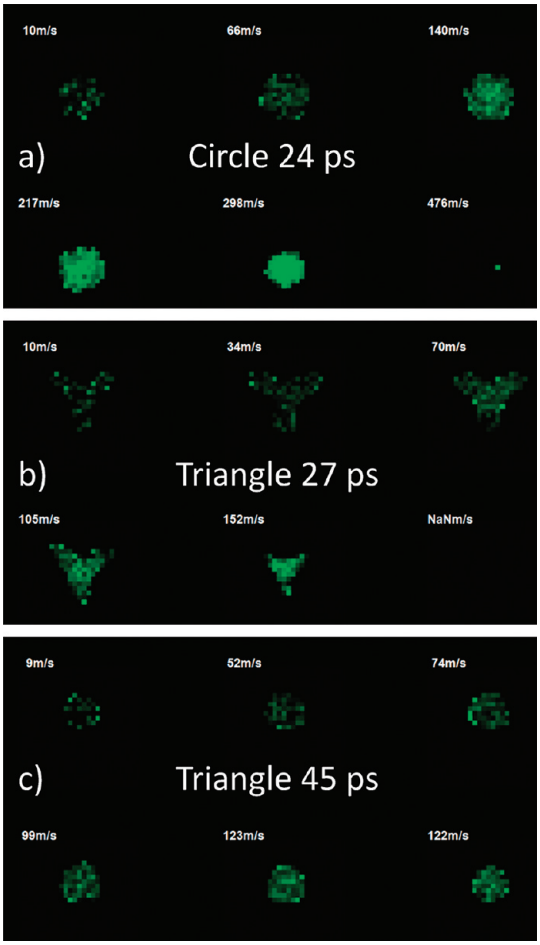

Figure 5. Color map (left-to-right and top-to-bottom) of the average atomic velocity as a function of height in 12 Å × 12 Å × 12 Å voxels at different *z*-slices at 1900 K: (a) circle at 24 ps; (b,c) equilateral triangle at 27 and 45 ps, respectively. Comparison of (a−c) reveals the velocity gradient in the *z*-dimension at the instant of nanodroplet coalescence, which for the circle happens coincidentally whereas for the equilateral triangle it happens in two-stages: initial coalescence of the edges at 27 ps (b) and final coalescence of the vertices at 45 ps (c). The result is a higher velocity gradient in the nanodroplet that resulted from the circle than in the nanodroplet that resulted from the equilateral triangle. This difference is ultimately reflected in the different velocities of the corresponding nanodroplets (see Figure 3).

ejection velocity. To illustrate the effect that temperature has on the traveling rim, Figure 6 shows the rim of the 1500 K (top) and 2200 K (bottom) circle at comparable retraction times (17 and 24 ps, left and right, respectively). The color map and velocity vectors indicate that at 2200 K the rim has larger vertical and radial velocities than at 1500 K. The average contact line displacements *versus* time were also calculated and interestingly revealed that the contact lines actually move at the same velocity and only diverge slightly as the droplet forms. From the pure viscosity change, it is surprising that the ∼37% change in viscosity would increase the nanodroplet velocity as much as it does, thus it is likely that subtle changes in the rim profile (where the viscous dissipation occurs) also contribute

TABLE 2. Calculated Temperature-Dependent Cu Properties

temperature (K)	surface energy (N/m)	viscosity (mPa·s)	density (g/cm^3)	# atoms for simulation
1500	1.273	4.288	7.884	33160
1700	1.231	3.825	7.724	32627
1900	1.190	3.496	7.564	31954
2200	1.127	3.149	7.324	30991

to the viscous losses (see, for instance, refs 23−26). The exact nature of the viscous and contact line losses will be studied in more detail in the future.

It is instructive to compare the temperature dependence of the ejection velocity found here to that found in ref 3. However, only qualitative comparisons are possible. This is because Habenicht *et al.*[3] investigated Au, whereas we have investigated Cu. They only investigated triangles, whereas we study triangles, squares, and circles. The size of the triangle they studied is much larger than the one we have studied: their triangle has a lateral size of 405 nm and a thickness of 95 nm, whereas ours has a lateral size of 32.3 nm and a height of 1 nm. Figure 3b in ref 3 showed the velocity dependence with the laser fluence but did not correlate laser fluence with the liquid temperature. The mass in ref 3 was constant, whereas in our simulations, the mass varies ∼7% between 1500 and 2200 K (on the other hand, the velocity should increase inversely with the square root of the mass, so the 7% mass change should be negligible). Despite all of these differences, a qualitative comparison between Habenicht *et al.*'s[3] results and ours immediately reveals a discrepancy: in Habenicht *et al.*,[3] the velocity is constant until a factor of about twice the critical fluence, F_C (the fluence to initiate jumping), at which point the velocity increases sharply. The increase in velocity at $\sim 2F_C$ was attributed to evaporative mass loss. We determined the evaporative mass loss for the 2200 K circle and found it to be negligible (only a few atoms evaporated during the droplet formation time). It is logical that our simulated mass loss would be much smaller as our liquid lifetimes are much shorter (200 ps) relative to their liquid lifetimes (likely tens of nanoseconds). Habenicht *et al.*[3] explained that the velocity remains constant because velocity is gained due to the conversion of surface energy into kinetic energy, and the amount converted is independent of the laser fluence. This explanation, however, neglects the temperature-dependent surface energy and viscous dissipation. It is possible that their fluence change is inducing smaller temperature changes than what we are simulating, or that the dimensional differences account for their onset of evaporation which our much smaller features do not observe. In any case, it is clear that the dependence of ejection velocity on temperature requires further studies.

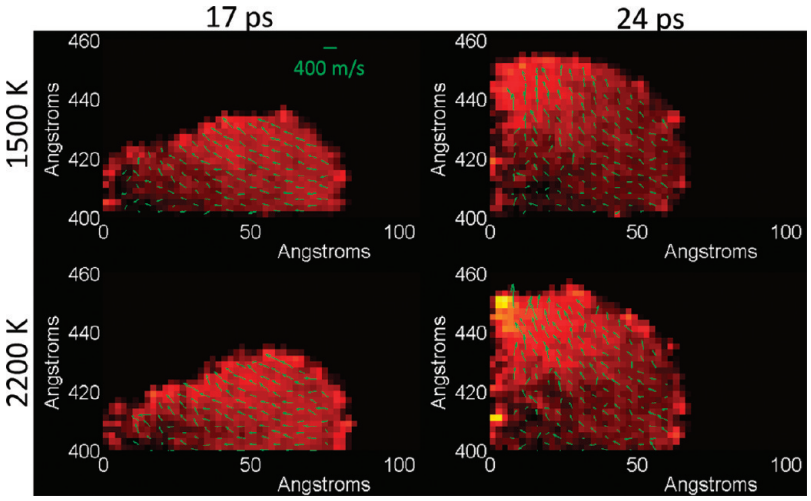

Figure 6. Cross-section velocity color maps with velocity vectors for two times of the dewettting, 17 and 24 ps, for the circle at 1500 and 2200 K, respectively. The increased velocity at 2200 K is attributed to a decreased viscosity in the Cu film and thus a decrease in the viscous dissipation.

CONCLUSIONS

Molecular dynamics simulations revealed that nanoscale liquid Cu nanostructures deposited on graphite dewet and coalesce into nanodroplets that are ejected with velocities that depend on their initial shape and temperature. The dependence of the ejected velocity on shape was ascribed to the temporal asymmetry of the mass coalescence during the droplet formation; the dependence on temperature was ascribed to changes in the density and viscosity. These results suggest that nanosecond laser pulses can be used to control the velocity of ejected nanoparticles. Indeed, such pulses have been used already to investigate the ejection of Au triangular shapes deposited on graphite/silica,[3,27] thus it should not be difficult to investigate other shapes, as well. Such an experiment will permit probing our findings and the explanations that we give for the trends we observe.

METHODS

The Cu liquid nanostructures in the shape of a circle, square, equilateral, and isosceles triangle, all with the same area (45238.9 Å^2) and thickness (10 Å), were extracted from a bulk liquid Cu. The liquid bulk was generated using an embedded atom method (EAM) potential[28,29] and made at different temperatures (*i.e.*, 1500, 1700, 1900, and 2200 K) using an isobaric–isothermal, NPT, ensemble. Subsequently, liquid Cu nanostructures in the shapes of circle, square, equilateral, and isosceles triangles were extracted from the bulk liquid and deposited on a graphitic substrate (see first row of Figure 1) composed of three layers. The top layer was fixed at the same temperature as the Cu nanostructure using a canonical, NVT, ensemble, whereas the remaining two layers were kept frozen. The graphitic substrate was described with an adaptive intermolecular reactive empirical bond order (AIREBO) potential,[30] and the minimum vertical distance between the Cu nanostructure and the top layer of the substrate was 3.225 Å. The interaction between Cu and C was described with a 12-6 Lennard-Jones potential with a well depth $\varepsilon = 0.010$ eV and size parameter $\sigma = 3.225$ Å. This is the same potential we used in ref 13. This LJ potential was found to reproduce the equilibrium contact angle of Cu on graphite (134° *versus* 140° experimentally[31]) and the binding energy of the Cu(111)/graphite interface (91.89 meV *versus* 35[32] and 38[33] meV as given by *ab initio* calculations based on the local density approximation, LDA, or the van der Waals density functional, vdW-DF, respectively) better than a similar LJ potential used by Huang *et al.*[34] Finally, a 200 ps MD simulation was carried out where the liquid Cu nanostructure was allowed to evolve freely while the top layer of the graphitic substrate was kept at constant temperature. The same methodology was used in ref 13 and proved to be appropriate. All the calculations were carried out with the software LAMMPS.[35]

It is important to consider the following assumptions regarding our model. First, the model of a solid geometry instantly converted into a liquid of the same shape closely mimics the fact that nanosecond/picosecond pulsed laser melting experiments produce ultrafast heating rates (10^9–10^{10} K/s). Nonetheless, it is important to note that in our simulations the temporal nature of the laser pulse is not considered, as the initial solid shape is treated as instantly molten. This means that our results can only be directly compared to those of Habenicht *et al.*[3] because in Huang *et al.*[4] melting does not occur. Second, the liquid temperature is treated as homogenously distributed, an assumption that Habenicht *et al.*[3] also made and which they based on the fact that the thermal diffusion length was considerably greater than the thickness of the sample. Third, in Habenicht *et al.*,[3] the substrate is at a lower temperature that the nanodroplet. As a result, nanodroplets not ejected from the substrate exchange heat with the substrate and resolidification ensues. In our simulations, the fixed substrate temperature prevents solidification.

Acknowledgment. The authors acknowledge support from the U.S. Department of Energy, Basic Energy Sciences, Materials Sciences and Engineering Division. B.H.R. was supported by an appointment under the Higher Education Research Experience (HERE) program, administered by the Oak Ridge Institute for Science and Education between the U.S. Department of Energy and Oak Ridge Associated Universities. M.F.C. acknowledges the computational resources of the UT/ORNL National Institute for Computational Sciences.

REFERENCES AND NOTES

1. Fennimore, A. M.; Yuzvinsky, T. D.; Han, W. Q.; Fuhrer, M. S.; Cumings, J.; Zettl, A. Rotational Actuators Based on Carbon Nanotubes. *Nature* **2003**, *424*, 408–410.

2. Whitesides, G. M. The Once and Future Nanomachine—Biology Outmatches Futurists' Most Elaborate Fantasies for Molecular Robots. *Sci. Am.* **2001**, *285*, 78–83.
3. Habenicht, A.; Olapinski, M.; Burmeister, F.; Leiderer, P.; Boneberg, J. Jumping Nanodroplets. *Science* **2005**, *309*, 2043–2045.
4. Huang, W.; Qian, W.; El-Sayed, M. A. Gold Nanoparticles Propulsion from Surface Fueled by Absorption of Femtosecond Laser Pulse at Their Surface Plasmon Resonance. *J. Am. Chem. Soc.* **2006**, *128*, 13330–13331.
5. Fitz-Gerald, J. M.; Pique, A.; Chrisey, D. B.; Rack, P. D.; Zeleznik, M.; Auyeung, R. C. Y.; Lakeou, S. Laser Direct Writing of Phosphor Screens for High-Definition Displays. *Appl. Phys. Lett.* **2000**, *76*, 1386–1388.
6. Guan, Y. F.; Pearce, R. C.; Melechko, A. V.; Hensley, D. K.; Simpson, M. L.; Rack, P. D. Pulsed Laser Dewetting of Nickel Catalyst for Carbon Nanofiber Growth. *Nanotechnology* **2008**, *19*, 235604.
7. Rack, P. D.; Guan, Y.; Fowlkes, J. D.; Melechko, A. V.; Simpson, M. L. Pulsed Laser Dewetting of Patterned Thin Metal Films: A Means of Directed Assembly. *Appl. Phys. Lett.* **2008**, *92*, 223108.
8. Kondic, L.; Diez, J. A.; Rack, P. D.; Guan, Y. F.; Fowlkes, J. D. Nanoparticle Assembly *via* the Dewetting of Patterned Thin Metal Lines: Understanding the Instability Mechanisms. *Phys. Rev. E* **2009**, *79*, 026302.
9. Fowlkes, J. D.; Wu, Y. Y.; Rack, P. D. Directed Assembly of Bimetallic Nanoparticles by Pulsed-Laser-Induced Dewetting: A Unique Time and Length Scale Regime. *ACS Appl. Mater. Interfaces* **2010**, *2*, 2153–2161.
10. Wu, Y. Y.; Fowlkes, J. D.; Rack, P. D.; Diez, J. A.; Kondic, L. On the Breakup of Patterned Nanoscale Copper Rings into Droplets *via* Pulsed-Laser-Induced Dewetting: Competing Liquid-Phase Instability and Transport Mechanisms. *Langmuir* **2010**, *26*, 11972–11979.
11. Wu, Y.; Fowlkes, J. D.; Rack, P. D. The Optical Properties of Cu−Ni Nanoparticles Produced *via* Pulsed Laser Dewetting of Ultrathin Films: The Effect of Nanoparticle Size and Composition on the Plasmon Response. *J. Mater. Res.* **2011**, *26*, 277–287.
12. Fowlkes, J. D.; Kondic, L.; Diez, J.; Wu, Y.; Rack, P. D. Self-Assembly *versus* Directed Assembly of Nanoparticles *via* Pulsed Laser Induced Dewetting of Patterned Metal Films. *Nano Lett.* **2011**, *11*, 2478–2485.
13. Fuentes-Cabrera, M.; Rhodes, B. H.; Fowlkes, J. D.; Lopez-Benzanilla, A.; Terrones, H.; Simpson, M. L.; Rack, P. D. Molecular Dynamics Study of the Dewetting of Copper on Graphite and Graphene: Implications for Nanoscale Self-Assembly. *Phys. Rev. E* **2011**, *83*, 041603.
14. Koplik, J.; Banavar, J. R. Molecular Simulations of Dewetting. *Phys. Rev. Lett.* **2000**, *84*, 4401–4404.
15. De Coninck, J.; Blake, T. D. Wetting and Molecular Dynamics Simulations of Simple Liquids. *Annu. Rev. Mater. Res.* **2008**, *38*, 1–22.
16. de Ruijter, M. J.; Blake, T. D.; De Coninck, J. Dynamic Wetting Studied by Molecular Modeling Simulations of Droplet Spreading. *Langmuir* **1999**, *15*, 7836–7847.
17. Bertrand, E.; Blake, T. D.; De Coninck, J. Dynamics of Dewetting at the Nanoscale. *Eur. Phys. J.* **2009**, *166*, 173–176.
18. Bertrand, E.; Blake, T. D.; Ledauphin, V.; Ogonowski, G.; De Coninck, J.; Fornasiero, D.; Ralston, J. Dynamics of Dewetting at the Nanoscale Using Molecular Dynamics. *Langmuir* **2007**, *23*, 3774–3785.
19. Blake, T. D.; Clarke, A.; De Coninck, J.; deRuijter, M. J. Contact Angle Relaxation During Droplet Spreading: Comparison between Molecular Kinetic Theory and Molecular Dynamics. *Langmuir* **1997**, *13*, 2164–2166.
20. Webb, E. B.; Grest, G. S.; Heine, D. R. Precursor Film Controlled Wetting of Pb on Cu. *Phys. Rev. Lett.* **2003**, *91*, 236102.
21. Heine, D. R.; Grest, G. S.; Webb, E. B. Surface Wetting of Liquid Nanodroplets: Droplet-Size Effects. *Phys. Rev. Lett.* **2005**, *95*, 107801.
22. Bian, X. F.; Zhang, J. X.; Jia, Y. B.; Sun, M. H. Viscosity Characteristic in Metallic Melts with Medium/Short-Range Order Structures. *Chin. Phys. Lett.* **2005**, *22*, 644–647.
23. Taylor, G. I.; Michael, D. H. Making Holes in a Sheet of Fluid. *J. Fluid Mech.* **1973**, *58*, 625.
24. Callegari, G.; Calvo, A.; Hulin, J. P. Experimental Results of Dewetting in the Visco-gravitational Regime. *Colloids Surf., A* **2002**, *206*, 167–177.
25. Andrieu, C.; Sykes, C.; Brochard, F. Dynamics of Fast Dewetting on Model Solid Substrates. *J. Adhes.* **1996**, *58*, 15–24.
26. Brochardwyart, F.; Degennes, P. G. Dynamics of Partial Wetting. *Adv. Colloid Interface* **1992**, *39*, 1–11.
27. Boneberg, J.; Habenicht, A.; Benner, D.; Leiderer, P.; Trautvetter, M.; Pfahler, C.; Plettl, A.; Ziemann, P. Jumping Nanodroplets: a New Route towards Metallic Nanoparticles. *Appl. Phys. A* **2008**, *93*, 415–419.
28. Daw, M. S.; Baskes, M. I. Semiempirical, Quantum-Mechanical Calculation of Hydrogen Embrittlement in Metals. *Phys. Rev. Lett.* **1983**, *50*, 1285–1288.
29. Daw, M. S.; Baskes, M. I. Embedded-Atom Method—Derivation and Application to Impurities, Surfaces, and Other Defects in Metals. *Phys. Rev. B* **1984**, *29*, 6443–6453.
30. Stuart, S. J.; Tutein, A. B.; Harrison, J. A. A Reactive Potential for Hydrocarbons with Intermolecular Interactions. *J. Chem. Phys.* **2000**, *112*, 6472–6486.
31. Naidich, Y. V.; Kolesnichenko, G. A. A Study of Wetting of Diamond and Graphite by Fused Metals and Alloys VII. The Effect of Vanadium, Niobium, Manganese, Molybdenum, and Tungsten on Wetting of Graphite by Copper-Based Alloys. *Powder Metall. Met. Ceram.* **1968**, *7*, 3.
32. Jones, R. O.; Gunnarsson, O. The Density Functional Formalism, Its Applications and Prospects. *Rev. Mod. Phys.* **1989**, *61*, 689–746.
33. Vanin, M.; Mortensen, J. J.; Kelkkanen, A. K.; Garcia-Lastra, J. M.; Thygesen, K. S.; Jacobsen, K. W. Graphene on Metals: A van der Waals Density Functional Study. *Phys. Rev. B* **2010**, *81*, 081408.
34. Huang, S. P.; Mainardi, D. S.; Balbuena, P. B. Structure and Dynamics of Graphite-Supported Bimetallic Nanoclusters. *Surf. Sci.* **2003**, *545*, 163–179.
35. Plimpton, S. Fast Parallel Algorithms for Short-Range Molecular-Dynamics. *J. Comp. Phys.* **1995**, *117*, 1–19.